Catalysis Today 169 (2011) 85–92

Contents lists available at ScienceDirect

Catalysis Today

journal homepage: www.elsevier.com/locate/cattod

Kinetic analysis of reduction of MoO_3 to MoO_2

Erwin Lalik*

Institute of Catalysis and Surface Chemistry, Polish Academy of Sciences, ul. Niezapominajek 8, 30-239 Krakow, Poland

ARTICLE INFO

Article history:
Available online 16 October 2010

Keywords:
MoO_3
MoO_2
Mo_4O_{11}
Reduction
Molybdenum
Kinetics

ABSTRACT

Two kinetic models have been proposed as alternative representations of reaction mechanism for the reduction of MoO_3 to MoO_2. An analytical solution of one of them as well as stochastic simulations of both models yielded results that could be compared to a set of very precise kinetic curves obtained experimentally using neutron diffraction *in situ* followed by multiphase Rietveld refinement of the resulting diffraction patterns. By a short margin, the results obtained from the model called the autocatalytic comproportionation seem to explain the experimental data better than the other model called the competitive nucleation. Implications as well as further applicability of the models are also discussed.

1. Introduction

The industrial extraction of metallic molybdenum powder is a stepwise process that begins with reduction of MoO_3 (or ammonium dimolybdate) to MoO_2 with gaseous hydrogen. Typically, the first stage of the reduction is carried out at 500–600 °C, followed by a second, high-temperature stage in which the MoO_2 is further reduced to metal, again by hydrogen, at 950–1100 °C. Powder metallurgy of molybdenum relies heavily on sintering, and so it is essential for the commercial viability of the Mo powder to have properties facilitating its use for the purpose. Yet technological difficulties in obtaining such properties seem to prevail in spite of extensive research. It has long been known from industrial practice that it is the first stage, i.e., the formation of MoO_2, which appears to be crucial for the sintering abilities of Mo powders to be satisfactory [1]. Technological errors at this early stage may impair the sintering capability of the final Mo-powder, resulting in defects such as cracks or blisters revealed after sintering. The second stage, featuring the high-temperature reduction of MoO_2 to Mo, seemed to be somehow less prone to technical adversities. However, recent results seem to suggest that the powder characteristics of the final Mo are also strongly dependent on its oxygen content, the latter determined during the second stage of reduction [2].

Reducibility of MoO_3 is also conducive to its applications in catalytic oxidation processes, and so the mechanism of its reduction has been widely studied since early sixties [1–25]. The reaction had been initially considered topotactic (direct MoO_3-to-MoO_2) [3,4], but this notion would soon be challenged by occasional detections of the Magneli phase γ-Mo_4O_{11} in the reaction mixture [5–7]. To account for the γ-Mo_4O_{11} intervention, a consecutive mechanism has been proposed, with γ-Mo_4O_{11} as an intermediate formed from MoO_3 and further transformed into MoO_2. However, subsequent studies using *in situ* XAS and XRD [22,23] suggested that γ-Mo_4O_{11} may be formed in a reaction of MoO_3 with MoO_2 rather than by reduction of MoO_3 with gaseous H_2. Such a pathway of γ-Mo_4O_{11} formation proposed by the authors of Refs. [22,23] involved nucleation as the rate controlling step, but this mechanism was questioned by the author of Ref. [24] on the ground that it did not account for the autocatalytic effect of MoO_2 previously observed for this reaction [6].

The kinetic curves obtained using neutron powder diffraction (NPD) *in situ* [25] confirmed the notion of γ-Mo_4O_{11} formation as a comproportionation of MoO_3 and MoO_2. Yet they also revealed a striking feature that has not been reported before, namely the plateau of the MoO_2 profile (cf. Fig. 1a), sustained for ca. 5 h. During this period the MoO_2 content does not change, in spite of the unabated MoO_3 consumption. In the present paper a mechanism is proposed that account for both the autocatalytic effect of MoO_2, as well as the formation of γ-Mo_4O_{11} from $MoO_3 + MoO_2$.

2. Data

The experimental data represent reduction of a 10 g sample (ca. 50 mm in height) of well crystalline MoO_3 at 550 °C with hydrogen (diluted with helium; H_2/He = 3/7) flowing-through at 30 cm^3/min. The kinetic curves for all three phases: MoO_3, MoO_2 and γ-Mo_4O_{11}, each consisting of 123 experimental points, have been obtained using neutron diffraction *in situ*, with the acquisition time of 10 min, over an experiment lasting ca. 23 h. The experimental conditions as well as the details of the multiphase Rietveld analysis of each

* Tel.: +48 12 6395189.
E-mail address: nclalik@cyf-kr.edu.pl.

0920-5861/$ – see front matter © 2010 Elsevier B.V. All rights reserved.
doi:10.1016/j.cattod.2010.09.013

of the 123 diffraction patterns have been given in Ref. [25]. Apart from the three phases mentioned above, only a negligible trace of η-Mo_4O_{11} has been detected at a moment during reduction. For brevity, subsequently Mo_4O_{11} is used for γ-Mo_4O_{11}.

3. Kinetic analysis

3.1. Model assumptions

3.1.1. Essential characteristics of the experimental kinetic curves

The kinetic curves representing the fractional contents vs. time for MoO_3, Mo_4O_{11} and MoO_2 can be seen in Fig. 1a (symbol curves). Four characteristics can be pointed out that are essential to these curves and have to be accounted for in proposing reaction mechanism. First, the content of MoO_2 is initially higher than that of Mo_4O_{11}. This is evident from the profiles of MoO_2 and Mo_4O_{11} during the first 2–3 h of the reaction (cf. Fig. 1b). It indicates that MoO_2 is a primary product of the reduction of MoO_3. Secondly, the initial build-up of MoO_2 unexpectedly comes to a standstill and for the next 5 h the MoO_2 content lingers at a level barely about 0.06, rather than continuing to grow. A prolonged plateau attained by the MoO_2 profile graphically demonstrates this astonishing development. The other two curves meanwhile continue their courses: the MoO_3 declining; the Mo_4O_{11} rising. This suggests that the reaction reaches a steady state in which MoO_2 is formed from MoO_3, but simultaneously converted to Mo_4O_{11} at the same rate. The build up

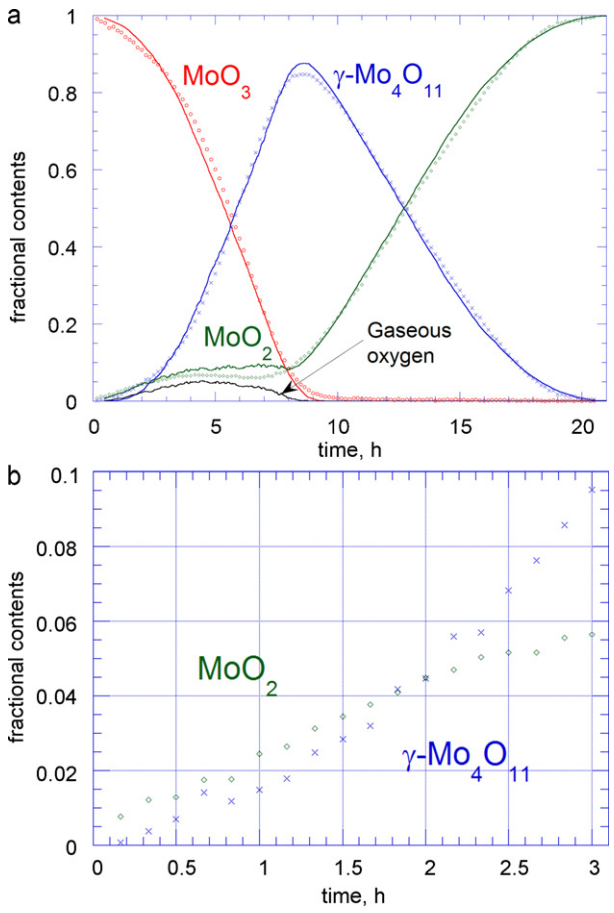

Fig. 1. (a) The symbols show experimental values of phase contents vs. time (kinetic curves) for MoO_3, MoO_2 and Mo_4O_{11} during the reduction of MoO_3 with H_2 at 550 °C. The solid lines represent the simulated kinetic curves for all the three solids and also for the gaseous oxygen (see Section 3.3). (b) Enlargement of the initial section of the experimental kinetic curves for MoO_2 (diamonds) and Mo_4O_{11} (crosses) showing that the MoO_2 is a primary product at this stage.

of MoO_2 resumes when MoO_3 is depleted, coinciding with a conspicuous maximum attained by the Mo_4O_{11} profile. The third key characteristic, therefore, is the bell-shaped profile of Mo_4O_{11} that confirms the intervening manner of the Mo_4O_{11} formation. Its maximum coinciding with the total depletion of MoO_3 indicates that in the concluding stage of the process, MoO_2 is being produced solely from the previously accumulated Mo_4O_{11}. Finally, all three curves have sigmoidal shape, which may be indicative of an autocatalytic character of some of the reactions they represent.

3.1.2. Formation of Mo_4O_{11} via comproportionation of MoO_3 and MoO_2

The content profiles in the first 8 h in Fig. 1a are reminiscent of a "classic" consecutive kinetics where an intermediate species reaches a plateau indicating that a steady state of the process is being achieved. In our case it is the MoO_2 that reaches the plateau suggesting a steady state of the following reaction sequence $MoO_3 \rightarrow MoO_2 \rightarrow Mo_4O_{11}$. But Mo_4O_{11} cannot be formed solely from MoO_2 in the reducing atmosphere of hydrogen. To be reoxidized, the MoO_2 needs oxygen, and the only source of oxygen in this system is MoO_3. Thus the only way for the Mo_4O_{11} to be formed is a comproportionation of MoO_3 with MoO_2, presumably following a topotactic formation of the latter from the starting MoO_3, and so the mechanism of reduction should involve at least two consecutive steps: $MoO_3 \rightarrow MoO_2$ and $MoO_3 + MoO_2 \rightarrow Mo_4O_{11}$. This is in agreement with the existing knowledge concerning the formation of Mo_4O_{11}. The latter is normally obtained from a mechanical mixture of MoO_3 and MoO_2 (or Mo) heated in an evacuated quartz tube at 600–800 °C [26]. In fact, Mo_4O_{11} failed to be formed from MoO_3 with gaseous hydrogen as reducing agent, but it has been formed by re-oxidation of MoO_2 under low partial pressure of oxygen [14,17] whereas under higher partial pressures MoO_2 has been oxidized directly to MoO_3 [27].

3.1.3. Oxygen transport for the Mo_4O_{11} formation

Fig. 2 shows that the formation of MoO_2 proceeds only in one crystallographic direction in MoO_3, so that the product does not cover the whole crystallite, but only its basal planes. According to the topotactic mechanism [4], the MoO_3/MoO_2 interface is formed parallel to the (0 1 0), the basal plane of the MoO_3 crystallite, and moves down along the [0 1 0] as the reaction progresses layer by layer, without changing the morphology [4,12,17]. Note that the basal (0 1 0) plane of the crystallite is parallel to the MoO_3 double layers, and is more pronounced than the side planes, (1 0 0) and (0 0 1). Such morphology is typical for the well-grown MoO_3 crystallites [28]. By the time that the formation of Mo_4O_{11} takes over the MoO_2 domains cover the (0 1 0) planes of MoO_3 crystallites, leaving however the side planes free.

With the side planes remaining exposed to the gas phase, there may be two conceivable ways for oxygen to be provided from MoO_3 to MoO_2 in order to form Mo_4O_{11}. First, the oxide anions may transfer directly across the MoO_3/MoO_2 interface, or, second, indirectly, the oxygen species on the exposed MoO_3 planes may desorb to the gas phase and be recaptured by MoO_2. The first possibility, although apparently a simpler one, seems less likely, since the formation of Mo_4O_{11} at the MoO_3/MoO_2 interface must create a spatial hindrance for diffusion of oxygen as the Mo_4O_{11} layer separating MoO_3 from MoO_2 would be growing thicker with the reaction progress. In such a case the growth of Mo_4O_{11} might be expected to obey the well-known parabolic law [29]. But this is not the case; the experimental Mo_4O_{11} profile in Fig. 1a is not parabolic. Instead, it is of sigmoid shape indicating, that rather than being slowed down the rate of Mo_4O_{11} formation actually increases with the reaction progress. We therefore propose that the formation of Mo_4O_{11} involves transport of oxygen through the gas phase. This concept is visualized in Fig. 2. Note that it involves diffusion of oxygen anions

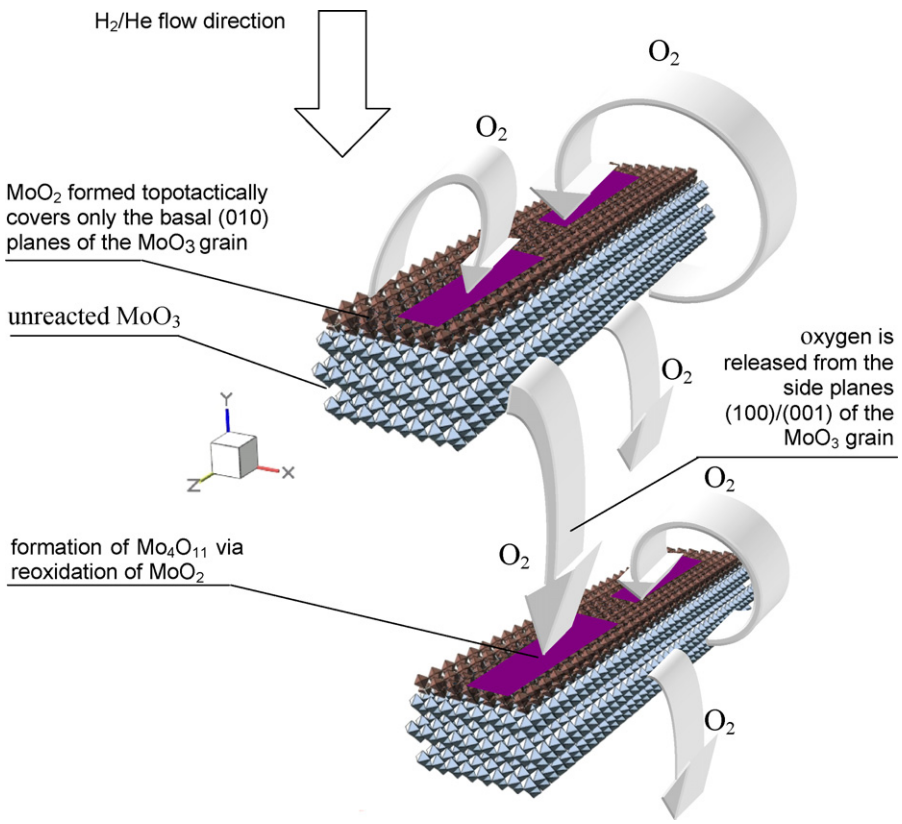

Fig. 2. The proposed mechanism of oxygen transport from MoO_3 to MoO_2 that may lead to the formation of Mo_4O_{11}. Typical morphology of MoO_3 crystallites shows well grown basal planes (0 1 0) parallel to double layers of the MoO_6 octahedra (grayish-blue). After an initial period of presumably topotactic reduction, these planes will be covered by MoO_2 domains (brown) parallel to the MoO_3 layers, with the side planes (1 0 0) and (0 0 1) remaining free. Two arbitrary crystallites undergoing reduction have been shown; for clarity only the top MoO_2 domain has been drawn; in reality both sides of the crystallites may be covered by MoO_2. Thermal decomposition of MoO_3 results in desorption of oxygen from the side planes of crystallites, since within the layered structure of MoO_3, the oxygen species diffuse from the bulk to the surface preferentially along the direction parallel to the layers (see Section 3.1). After desorption gaseous oxygen can deoxidize the MoO_2 domains of both the same as well as of the neighboring crystallites to form Mo_4O_{11} (purple).

in a direction parallel rather than perpendicular to the MoO_3 layered structure. The activation energy for such a parallel migration is lower compared to that for a perpendicular diffusion (0.5 eV and 0.9 eV respectively) [30] and hence the anisotropy of the solid diffusion of oxygen species seems to facilitate the apparently more complex mechanism of Mo_4O_{11} formation involving desorption of oxygen from MoO_3.

Also the role of MoO_3 morphology has been confirmed by comparison of the rates of the isotope exchange between the gaseous $C^{18}O_2$ and the different planes of crystalline $Mo^{16}O_3$ [31]. Samples exposing predominantly the lateral (1 0 0)/(0 0 1) faces appeared to exchange oxygen faster than those exposing mainly the (0 1 0) faces at 500 °C, when the diffusion of oxygen species through the solid was involved. By contrast, at 350 °C, when diffusion was slow and only the surface was involved in the exchange, the (0 1 0)-reach samples turned out to be more active. The authors of Ref. [31] have pointed out, that it may be the preferential migration of oxygen species parallel to the layers that makes the side faces of MoO_3 crystallites more active in the isotope exchange at higher temperature. The "higher temperature" here should mean in excess of 400 °C. It has been observed by *in situ* HREM that at the temperature of 400 °C the mobility of the crystal lattice of MoO_3 (and molybdates) increases abruptly [32]. It should be therefore sufficiently high at 550 °C to support a rapid migration of anions within the oxygen sublattice of MoO_3. Assuming the topotactic reduction, a distance of this migration of oxygen anions within MoO_3 crystallites does not change during the process. Hence any influence of diffusion limitations on the rate of formation of Mo_4O_{11} should be approximately invariant during the reaction, so effectively it may be included in the reaction rate constant.

It should be noticed, that a mechanism of the formation of Mo_4O_{11} from MoO_3 that crucially depends on a transport through the gas phase has been proposed previously (at 550 °C in H_2) [33]. It was originally called the "chemical vapour transport" (CVT) and the suggestion was based on *ex situ* observations of a reaction mixture of the MoO_3 and the Mo_4O_{11} grains using electron scanning microscopy. However, the authors of Ref. [33] did not specify the nature of species transported via CVT in their experiments.

3.2. Kinetic mechanism

3.2.1. Autocatalytic comproportionation

Considering both the autocatalytic action of MoO_2 and the transport of oxygen through the gas phase being involved in the Mo_4O_{11} formation, we propose the following model of the reduction:

$$MoO_3 + MoO_2 + H_2 \xrightarrow{k_0} 2MoO_2 + H_2O \quad \text{autocatalytic} \quad (1)$$

$$MoO_3 + MoO_2 \xrightarrow{k_1} 2MoO_2 + 0.5O_2 \quad \text{autocatalytic} \quad (2)$$

$$4MoO_2 + 1.5O_2 \xrightarrow{k_2} Mo_4O_{11} \quad (3)$$

$$Mo_4O_{11} + 3H_2 \xrightarrow{k_3} 4MoO_2 + 3H_2O \quad (4)$$

The Eq. (1) represents the topotactic conversion of MoO_3 into MoO_2. This is accompanied by the vacuum-driven autocatalytic decomposition of MoO_3 (2). The oxygen released from MoO_3 in the reaction (2) is recaptured by MoO_2 and so the Mo_4O_{11} is formed (3).

Table 1
Reaction parameters for the model of autocatalytic comproportionation. Initial content of A has been set as 0.1 mol.

	Reactions	(21)	(22)	(23)	(24)
	Rate constants (mol/s)	1.3	78	130	26
Species	Molecular densities (mol/dm^3)	Reaction orders			
A	3.2	1	1	–	–
B	48.9	1	1.3	1	0.55
C	7.3	–	–	–	0.35
O	0.016	–	–	0.0–1.0	–

Finally, the accumulated Mo_4O_{11} is reduced by hydrogen back into the MoO_2 as represented by Eq. (4). The steps (2) and (3), therefore, represent the comproportionation. The overall stoichiometry, $MoO_3 + H_2 = MoO_2 + H_2O$, can be obtained by adding the Eqs. (1)–(4) with coefficients of the reaction (2) tripled.

Following the procedure developed in classic kinetics of chemical reactions, we denote the contents as follows: $[MoO_3] = x$; $[MoO_2] = y$; $[Mo_4O_{11}] = z$. As a first approximation, it is being assumed that the reactions (1)–(4) are first order in each oxide reactant meaning that in writing the rate equations, the exponents at the content factors x, y and z are all set to unity. The validity of this assumption can be checked against the results of stochastic simulations (cf. Table 1). It can be seen that the reaction orders of the oxide reactant are indeed mostly close to unity, except for the Mo_4O_{11} in the step (24), which corresponds to the reaction (4). But the simulations also show that this is a relatively slow reaction (cf. the rate constant for the step (24) in Table 1) and it only becomes a dominating reaction in the last stage of the reduction process. The rate equations for the reactions (1)–(4) are as follows:

$$\frac{dx}{dt} = -k_0xy - k_1xy = -(k_0 + k_1)xy \tag{5}$$

$$\frac{dy}{dt} = (k_0 + k_1)xy - k_2y + k_3z \tag{6}$$

$$\frac{dz}{dt} = k_2y - k_3z \tag{7}$$

The rate law for MoO_3 is defined by the reactions (1) and (2), in which MoO_3 is being used up, so that the right hand side of Eq. (5) consists of two terms taken with negative signs. Since both the reactions are autocatalytic, the rate of MoO_3 consumption, dx/dt, is proportional to the content of MoO_2 as well as to that of MoO_3 itself. The same two terms appear again on the right-hand side of the Eq. (6) expressing the rate law for MoO_2, but this time they are both taken as positive, since in the reactions (1) and (2) MoO_2 is being formed. The same goes for the reaction (4), so that the term containing content of Mo_4O_{11} is also positive. In reaction (3), however, MoO_2 is consumed, reoxidized by gaseous oxygen. The corresponding term is therefore negative, but apart from the MoO_2 content (y) this term should also contain a factor representing the oxygen partial pressure p_O. By assuming that the rate law is zero-order with respect to oxygen (zero exponent at p_O) we effectively put this partial-pressure factor to equal unity. While clearly an approximation, this is justified to the extent that many heterogeneous-oxidation reactions are of fractional order in oxygen, so that in many cases the rate is weakly dependent on partial pressure of the gaseous reagent. In reality the reaction (3) will probably be fractional order in oxygen and not, strictly speaking, zero-order. But such an error being rather small, this approximation makes it possible to find an analytical solution to the system. The rate law for Mo_4O_{11} is defined by the reactions (3) and (4) in a similar way resulting in Eq. (7). The reactions (1) and (4) both involve gaseous hydrogen, but the partial pressure of hydrogen was kept constant throughout the reduction so that its representation factors are also constant, irrespective of their order(s), and as such are effectively included in the respective rate constants k_0 and k_3.

3.2.2. The steady state approximation

As the content of MoO_2 reaches a plateau (Fig. 1a), the steady state approximation can be applied to the content of MoO_2, so that $dy/dt = 0$, and consequently from Eq. (6) we find

$$y = \frac{k_3z}{k_2 - (k_0 + k_1)x} \tag{8}$$

Substitution of Eq. (8) into the rate Eqs. (5) and (6) gives

$$\frac{dx}{dt} = -\frac{dz}{dt} = -\frac{(k_0 + k_1)k_3xz}{k_2 - (k_0 + k_1)x} \tag{9}$$

Assuming $k_2 \gg (k_0 + k_1)$ we can neglect the second term in the denominator and write

$$\frac{dx}{dt} = -\frac{dz}{dt} \cong -\frac{(k_0 + k_1)k_3xz}{k_2} \tag{10}$$

The above inequality means that the reaction (3) is much faster than the reactions (1) and (2), which at this stage is an arbitrary assumption, but it is justified by the results obtained. Also, it seems to be confirmed by the results of stochastic simulations (cf. Table 1) showing that the rate constant for the step (23), which corresponds to k_2 in the model 1–4, is indeed the highest. To solve Eq. (10) we define the reaction variable a as the decrease in amount of MoO_3 in time t, so that

$$x(t) = x_0 - a(t) \tag{11}$$

where x_0 is the content of MoO_3 at the beginning of the reaction, $t_0 = 0$, and using the mass balance

$$x(t) + y(t) + z(t) = 1 \tag{12}$$

we can express z as

$$z(t) = a(t) + 1 - y_{ss} - x_0 \tag{13}$$

where y_{ss} denotes the content of MoO_2 at the steady state. On differentiation of Eqs. (11) and (13) we have

$$-\frac{dx}{dt} = \frac{dz}{dt} = \frac{da}{dt} \tag{14}$$

and for $x_0 = 1$ we can rewrite Eq. (10)

$$\frac{da}{dt} = k(1 - a)(a - y_{ss}) \tag{15}$$

where

$$k = \frac{(k_0 + k_1)k_3}{k_2} \tag{16}$$

Eq. (15) is an example of the so-called logistic equation. In the area of solid state kinetics, the logistic equations have been previously proposed, though without derivation, for autocatalytic decomposition [34] as well as for autocatalytic reduction [35].

3.2.3. Analytical integration

On separation of variables in Eq. (15) we obtain

$$\int_{a_1}^{a} \frac{da}{(1 - a)(a - y_{ss})} = \int_{t_1}^{t} k\,dt \tag{17}$$

for $1 > a > y_{ss}$, and integration from a fixed point $a_1 = 1 - x_1$ at the time t_1 to the variable upper limit a (x_1 is the MoO_3 content corresponding to beginning of the steady state period, that is MoO_2 plateau) yields

$$\frac{1}{1 - y_{ss}} \ln \frac{x(1 - y_{ss} - x_1)}{x_1(1 - y_{ss} - x)} = -k(t - t_1) \tag{18}$$

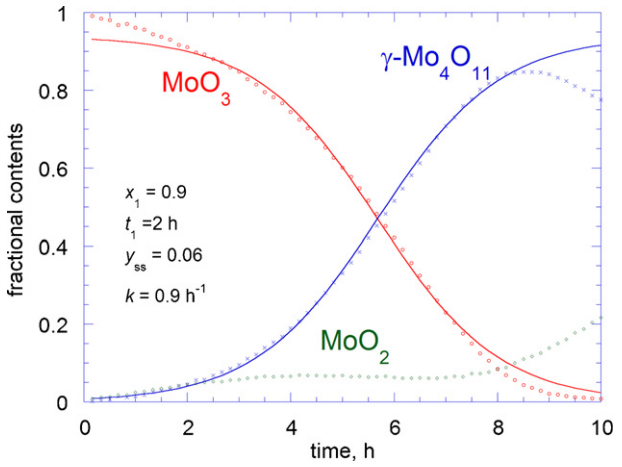

Fig. 3. Comparison of the plots calculated from Eqs. (19) and (20) (solid lines), for initial values $x_1 = 0.9$, $t_1 = 2$ h and $y_{ss} = 0.06$ (see Section 3.2), to the experimental content-vs.-time profiles of MoO_3 and Mo_4O_{11} in the steady state period (experimental profile of MoO_2 has also been showed).

from which we find the following expression for the content of MoO_3 as a function of time during the steady state period

$$x = \frac{1 - y_{ss}}{1 + ((1 - x_1 - y_{ss})/x_1)e^{(1-y_{ss})k(t-t_1)}} \quad (19)$$

and in similar manner for the content of Mo_4O_{11} as a function of time in the steady state we find

$$z = \frac{1 - y_{ss}}{1 + (x_1/(1 - x_1 - y_{ss}))e^{-(1-y_{ss})k(t-t_1)}} \quad (20)$$

The contents x and z are both sigmoidal functions of time. To fit our experimental data we take a mean MoO_2 content over the steady state period, $y_{ss} = 0.06$, and from Fig. 1a we find $x_1 = 0.9$ at $t_1 = 2$ h. Fig. 3 shows that the analytical expressions (19) and (20) fit well the experimental curves for both the MoO_3 and the Mo_4O_{11} respectively, within the steady state period, and we find an apparent first-order rate constant $k = 0.9\ h^{-1}$.

3.3. Stochastic simulations

Relying crucially on the steady state approximation, the analytical solution proposed in the preceding part is restricted to the period of the reduction in which the MoO_2 content can be considered constant. In order to model the whole extent of the reaction we have used the stochastic Monte Carlo modeling method implemented in Chemical Kinetic Simulation program (Version 1.01) available from IBM. While the fact that it is possible to fit the kinetic curves with an analytical solution does support the comproportionation mechanism, it does not constitute a definite proof that this mechanism is really in operation. We therefore attempted to widen the scope of modeling and considered an alternative mechanism, called the competitive nucleation, to be applied for the process of MoO_3 reduction. The competitive nucleation mechanism has been previously proposed in Ref. [36].

3.3.1. Simulation of autocatalytic comproportionation

The model has been formulated as follows:

$$A \Rightarrow B \quad (21)$$

$$A + B \Rightarrow 2B + O \quad (22)$$

$$3O + 4B \Rightarrow C \quad (23)$$

$$C + B \Rightarrow 2B \quad (24)$$

Table 2
Reaction parameters for the model of competitive nucleation. Initial content of A has been set as 0.1 mol.

Reactions	(25)	(26)	(27)	(28)
Rate constants (mol/s)	0.003–0.096	0.003	0.240	0.060

Species	Molecular densities (mol/dm^3)	Reaction orders			
A	3.2	1	1	1	–
B	48.9	–	–	–	1
C	7.3	–	–	1	1

where $A \equiv MoO_3$, $B \equiv MoO_2$, $C \equiv Mo_4O_{11}$, $O \equiv 1/2O_2$, and the parameters are presented in Table 1.

Fig. 4 shows that the simulation of this model reproduces well our experimental curves as seen in Fig. 1a. It also shows that the shape of the MoO_2 plateau is determined by the order of reaction in oxygen. The model that best resembles the experimental curves is when the order in oxygen is 0.54, and this is represented as solid lines in Fig. 1a, in agreement with our previous assumption concerning the fractional order of reaction with respect to oxygen.

3.3.2. Simulation of competitive nucleation

The second simulated mechanism has been the competitive nucleation [36,37]. Kinetically the nucleation is indistinguishable from autocatalysis, both producing characteristic sigmoid shape of kinetic curves. Since it is impossible to account for nucleation as such neither in the reaction equation nor in the rate law equation, therefore in simulation we considered the nucleation reactions as though they were autocatalytic. The model can be written as follows:

$$A \Rightarrow B \quad (25)$$

$$A \Rightarrow C \quad (26)$$

$$A + C \Rightarrow 2C \quad (27)$$

$$C + B \Rightarrow 2B \quad (28)$$

($A \equiv MoO_3$, $B \equiv MoO_2$, $C \equiv Mo_4O_{11}$) and the reaction parameters are shown in Table 2. The reactions (27) and (28) represent the consecutive reaction with *C* being an intermediate. Both steps have been assumed to involve nucleation/autocatalysis, so that in both cases the product, *C* in (27) and *B* in (28), appears in both sides of the reaction equations. A competing process is the direct formation of *B* from *A* as represented by reaction (25). The step (26) is added in order for the reaction (27) to kick off, alternatively some very small initial content of *C* could have been used, but including the additional step (26) seems to be more realistic. Fig. 5 represents the results of simulation in which the rate constant of the reaction (25) has been varied from 0.003 to 0.096 mol/s. The simulated kinetic curves reproduce well the intermediary manner of *C*, but less well the plateau of *B*. In fact, the *B* curve is always increasing, the rate of this increase being strongly dependent on the rate constant of the noncatalytic step (25).

4. Discussion

We have proposed and discussed two mechanisms that can account for the shape of our experimental kinetic curves: the autocatalytic comproportionation and the competitive nucleation.

4.1. Autocatalytic comproportionation

In view of the model of autocatalytic comproportionation the reduction of MoO_3 to MoO_2 would be proceeding through three distinctive periods: first, the topotactic MoO_3/MoO_2 conversion; second, the comproportionation of MoO_3 and MoO_2 to form

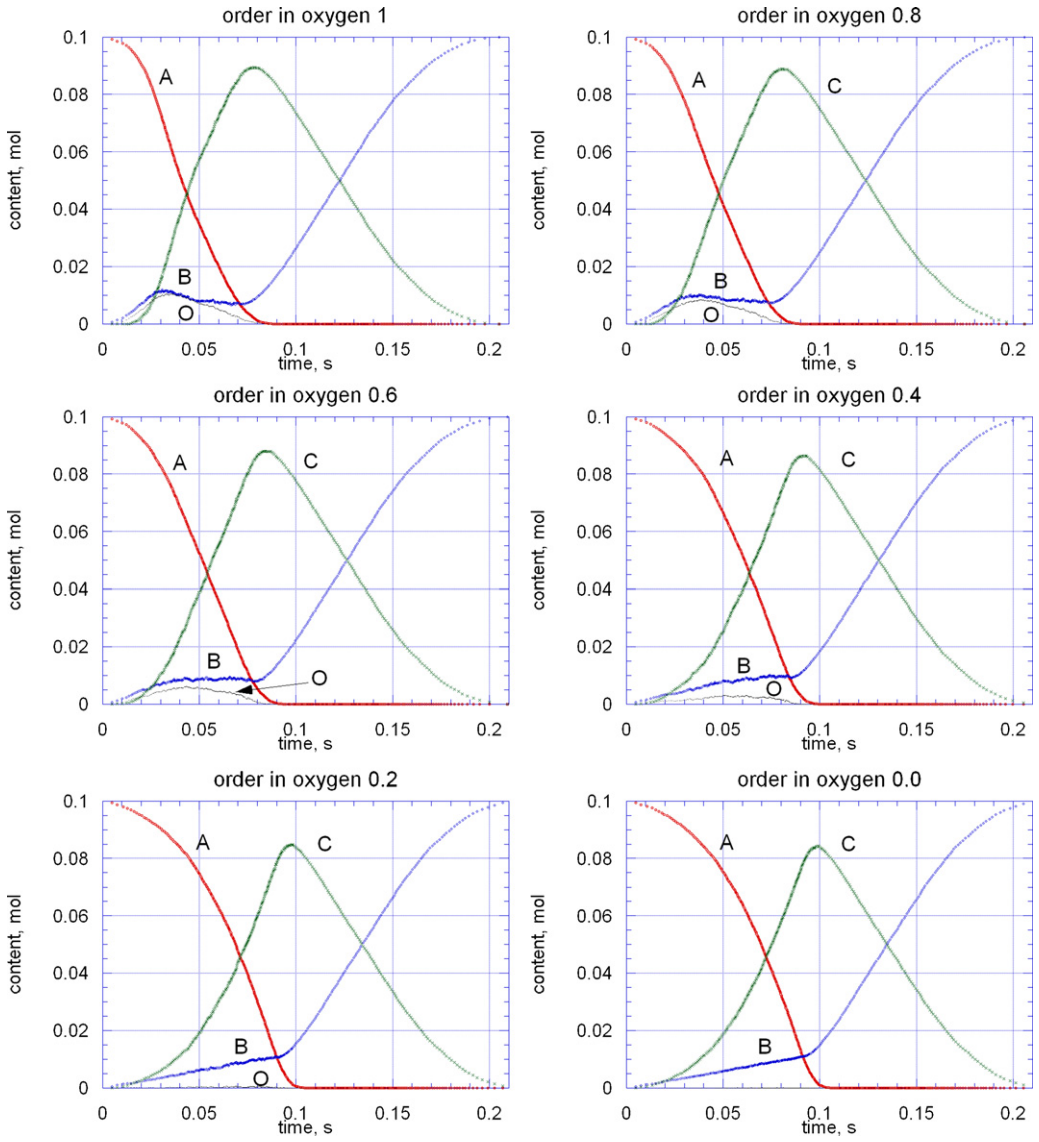

Fig. 4. Simulated kinetic curves of autocatalytic comproportionation (21–24), with the variable order of reaction (23) in oxygen, reproduce best the experimental profiles of MoO_3 reduction (see Fig. 1a) when the order in oxygen is set 0.4–0.6.

Mo_4O_{11}; third, reduction of Mo_4O_{11} to MoO_2. The first period serves also as an incubation of the autocatalytic effect showed by the topotactically formed MoO_2, possibly consisting of electron transfer from the MoO_2 phase to the MoO_3 across the interface (cf. next paragraph). This may facilitate the oxygen release from the MoO_3 surface, and by the onset of the second period an adventitious vacuum-driven reduction (decomposition) of MoO_3 grows up to accompany the hydrogen reduction. The oxygen released in the vacuum-driven reduction is recaptured by the topotactically formed MoO_2 domains, where Mo_4O_{11} is being formed. Thus the comproportionation grows up as a by process of the topotactic reduction before taking over in the second period. By the end of the second period, the MoO_3 that has served as an oxygen source for the comproportionation becomes depleted, and it takes the third period to entirely reduce the accumulated Mo_4O_{11} back into MoO_2. Therefore, the formation of Mo_4O_{11} in the course of reduction, as well as the notion of a direct (topotactic) transition from MoO_3 to MoO_2, can both be reconciled within a single kinetic model.

The autocatalytic action of MoO_2 can be envisaged as consisting of electron transfer to MoO_3 surface across the MoO_2/MoO_3 interface. On the topotactic reduction an interface between MoO_3 and MoO_2 must be formed as the reaction proceeds within a single grain or crystallite [4,17]. Because of difference of the work function, the electron transfer will take place across such interfaces from the MoO_2 phase to the MoO_3, as the latter has the higher value of work function (lower Fermi level). This will result in the formation of the so-called accumulation layer, that is an excess of the negative charge at the surface of MoO_3, and consequently in a downward bending of the energy bands at the surface [21,38]. With the lower edge of the conduction band shifted downward below the Fermi level, the extra electrons from MoO_2 will populate the low-laying levels within this band. As MoO_3 is a d^0 oxide, the lower part of its conduction band consists of antibonding Mo–O orbitals of mainly Mo 4*d* character [39]. Population of the antibonding Mo–O orbitals will result in a decreasing of bond energy, and thereby a weakening of the Mo–O bonds at the surface. It becomes, therefore, easier to break the Mo–O bond and to release oxygen from the surface.

The notion of desorption of oxygen from MoO_3 may help to rationalize some phenomena, which have been reported in relation to the reduction of MoO_3, yet seem to be insufficiently explained. First, we would like to mention an early observation of a moving front between different colorations across the static bed of MoO_3

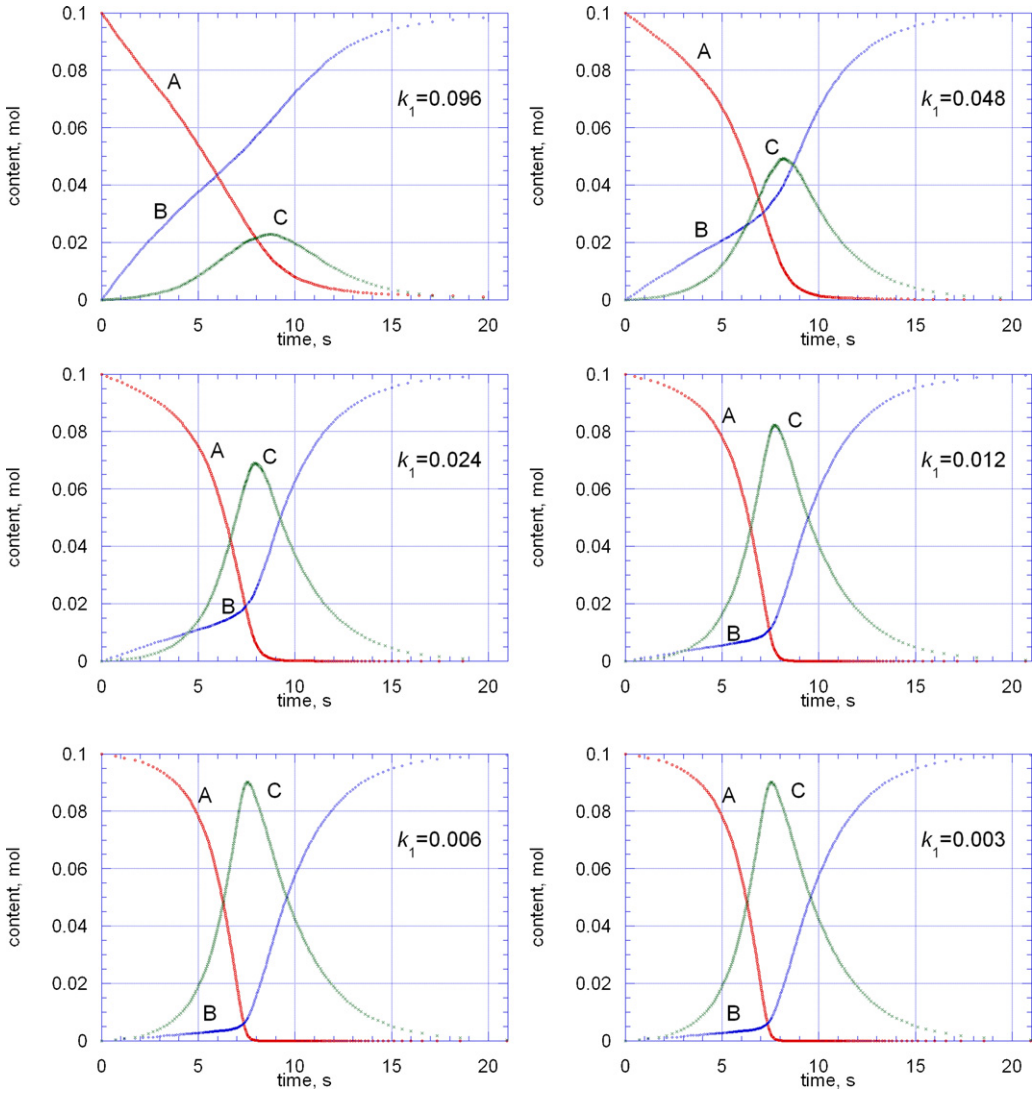

Fig. 5. Simulated kinetic curves of competitive nucleation (25–28), with variable rate constant k_1 of reaction (25).

on reduction [8,11]. This has been visually observed as a gradual change of colour travelling along the powder bed of MoO_3 in the direction parallel to the flow of hydrogen during reaction [11]. Yet the formation of the moving colour fronts cannot be explained by any gradients of partial pressure of a reducing agent along the bed. With the bed as short as 0.4 cm [11], the slow reduction taking hours to complete, and with the relatively fast flow of hydrogen, any decrease of pressure of hydrogen due to its consumption along the bed must indeed be absolutely negligible. In other words, all the MoO_3 grains will always experience the same pressure of hydrogen, so there is no reason for any grain to react with hydrogen faster than the others, irrespective of location within the bed. However, the oxygen released from MoO_3 at the top of the bed may travel down in the direction of hydrogen flow and be "recaptured" in the lower parts. Doing so it would be slowing down the reduction in those lower parts of the bed, and might be therefore responsible for the front formation.

The second phenomenon is a catalytic action of noble metals. It has been noticed that the reduction of MoO_3 by hydrogen can be accelerated by a mechanical admixture of platinum black prior to a gravimetric experiment [6]. The effect has been explained in terms of a spill-over of the dissociated hydrogen species from Pt, but the spill-over does not account for the fact that the catalytic action of Pt does not persist longer that the initial part of reduction, roughly not beyond the reduction degree of 0.4–0.5 [6]. But on the other hand, with its well established ability of dissociative adsorption of hydrogen, platinum is also an excellent catalyst of water formation from a gaseous mixture of O_2 and H_2. We suggest, therefore, that platinum black may very successfully compete with MoO_2 in recapturing gaseous oxygen released from the reduced MoO_3. That way it would effectively prevent the retention of oxygen in the solid, using the O_2 species to form the immediately desorbing H_2O rather than the Mo_4O_{11}. But the platinum black can act like this as long as there are O_2 molecules available, that is until the depletion of MoO_3, which in our experiment takes place at the reduction degree of approximately 0.4. Hence the depletion of MoO_3 as a source of gaseous oxygen would account for the observed, "premature" deactivation of the platinum black.

Perhaps this rationalization of the platinum effect may also help to explain the controversy mentioned in the Introduction between the authors of Refs. [6,24] and [22,23] respectively. In his response [40] to the comments in Ref. [24], the author of Ref. [39] has been rather dismissive about the catalytic effect of noble metals used in Ref. [24] as one of important arguments supporting the notion of Mo_4O_{11} formed solely from MoO_3 with the Pt facilitating the H_2 dissociation. However, within the framework of autocatalytic comproportionation, both the Pt effect and the formation of Mo_4O_{11} from $MoO_3 + MoO_2$ can be explained in terms of the same model.

4.2. Competitive nucleation

In view of the model of competitive nucleation there are two competitive pathways of the MoO_2 formation: the direct conversion of MoO_3, and the formation of MoO_2 in a consecutive manner with Mo_4O_{11} as an intermediate. The latter process may be autocatalytic or very sensitive to nucleation, which would explain the sigmoidal shape of kinetic curves. The model can account for some features of the experimental kinetic profiles (Fig. 1a), namely the bell-shape of the Mo_4O_{11} curve, and the fact that content of MoO_2 is initially higher than that of Mo_4O_{11}. The latter may be explained as a result of the autocatalytic (or sensitive to nucleation) manner of the Mo_4O_{11} formation from MoO_3, as the rate of this reaction, initially slow, may increase (autocatalytically) with rising Mo_4O_{11} content to eventually "overtake" the direct production of MoO_2 from MoO_3. However the MoO_2 plateau is not explained by competitive nucleation. In terms of this model, MoO_2 once formed does not undergo any further transformations; in particular it is not consumed so that its formation cannot reach a steady state and therefore the MoO_2 content should only be rising during the process; as it indeed has been showed to be the case by the simulation.

It should be noted, however, that although the competitive nucleation appears to be less consistent with the MoO_3 reduction, nevertheless the simulations of this mechanism yielded a category of profiles that may be consistent with certain other reactions, in particular, with a process for which this mechanism had been originally proposed; that is, with the hydration of cements [41]. Note that for a small reaction rate constant for the step (25), the content of *B* remains negligibly small during the initial period of simulated reaction. In practical experimentation, with this mechanism in operation, it might be difficult to detect such small content of a product. As a result, the practical kinetic profiles may show a large time lag, looking as though the formation of *B* started only at the point of maximum *C* rather than at the beginning of the process. Apart from the cement hydration [41], the experimental profiles featuring such a time lag have also been obtained for the reduction of CuO (supported on ZnO) to Cu metallic with Cu_2O as an intermediate [42].

5. Conclusions

A mechanism for the reduction of MoO_3 to MoO_2 has been proposed that seems to account for all major features observed for this reaction over nearly half of a century of investigations into this system. In particular, the mechanism called the autocatalytic comproportionation is able to account for a plateau in the curve representing the MoO_2 content in the solid reaction mixture of MoO_3, MoO_2 and Mo_4O_{11}, a surprising feature that has only been revealed using neutron powder diffraction for monitoring *in situ* the progress of reduction. Using both the analytical integration and the stochastic simulations of the model it was possible to reproduce the experimental kinetic curves in remarkable detail. The other model, the so called competitive nucleation that was also used for the stochastic simulations turned out to be less successful in reproducing the kinetic curves for the reduction of MoO_3, but it did show a potential to be applied for other reactions, including the hydration of cement, for which it originally had been proposed.

References

[1] E.R. Braithwaite, in: E.R. Braithwaite, J. Haber (Eds.), Molybdenum: An Outline of Its Chemistry and Uses, Studies in Inorganic Chemistry, vol. 19, Elsevier, Amsterdam, 1994, p. 20 (Chapter 1).
[2] G.P. Martins, T. Kangsadan, G. Scott, C. Wagner, J. Van Hoose, Mater. Sci. Forum 561–565 (2007) 447.
[3] M.J. Kennedy, S.C. Bevan, J. Less Common Met. 36 (1974) 23.
[4] L.C. Dufour, O. Bertrand, N. Floquet, Surf. Sci. 147 (1984) 396.
[5] A. Ueno, Y. Kotera, S. Okuda, C.O. Bennet, Proc 5th Int. Conf. Climax, 1982, p. 250.
[6] J. Sloczynski, W. Bobinski, J. Solid State Chem. 92 (1991) 436.
[7] R.J. Burch, Chem. Soc. Faraday Trans. 174 (1978) 2982.
[8] J. von Destinon-Forstmann, Can. Metall. Q 4 (1965) 1.
[9] L.A. Bursill, Acta Crystallogr. A 28 (1972) 187.
[10] L.A. Bursill, W.C.T. Dowell, P. Godman, N. Tate, Acta Crystallogr. A 34 (1977) 296.
[11] J. Orehotsky, L. Jamiolkowski, J. Gerboc, Mater. Sci. Eng. 41 (1979) 237.
[12] K.H. Carpanter, C.J. Hellada, in: P.C. Barry, C.H. Mitchell (Eds.), Proceedings, Climax 3rd International Conference on the Chemistryand Uses of Molybdenum, Ann Arbour, 1979, p. 204.
[13] P.L. Gai, Philos. Mag. A 43 (1981) 841.
[14] P.L. Gai, P.A. Labun, J. Catal. 94 (1985) 79.
[15] L.E. Firment, A. Faretti, Surf. Sci. 129 (1983) 155.
[16] J.M. Dominuez-Esquivel, S. Fuentes-Moyado, G. Diaz-Guerrero, A. Vazquez-Zavala, Surf. Sci. 175 (1986) L701.
[17] A. Anderson, S. Hansen, J. Solid State Chem. 75 (1988) 225.
[18] P.A. Spevack, N.S. McIntyre, J. Phys. Chem. 96 (1992) 9029.
[19] R.L. Smith, G.S. Rohrer, J. Catal. 163 (1996) 12.
[20] A. Kuzmin, J. Purans, Ph. Parent, H. Dexpert, J. Phys. IV France 7 (1997) C2–891.
[21] J. Haber, E. Lalik, Catal. Today 33 (1997) 119.
[22] T. Ressler, R.E. Jentoft, J. Wienold, M.M. Günter, O. Timpe, J. Phys. Chem. B 104 (2000) 6360.
[23] T. Ressler, R.E. Jentoft, J. Wienold, O. Timpe, J. Synchrotron Radiat. 8 (2001) 683.
[24] J. Sloczynski, J. Phys. Chem. B 106 (2002) 7718.
[25] E. Lalik, W.I.F. David, P. Barnes, J.F.C. Turner, J. Phys. Chem. B 105 (2001) 9153.
[26] L. Kihlborg, Adv. Chem. Ser. 39 (1963) 37.
[27] C. Kahruman, I. Yusufoglu, E. Oktay, Trans. Inst. Min. Metall. (Sect. C: Miner. Process. Extr. Metall.) 108 (1999) C8.
[28] L. Kihlborg, Ark. Chem. 21 (1963) 357.
[29] H. Schmalzried, Solid State Reactions, Verlag Chemie, Weinheim, 1981, p. 107.
[30] W. Thöni, P.B. Hirsch, Philos. Mag. 33 (1976) 639.
[31] A. Guerrero-Ruiz, I. Rodríguez-Ramos, P. Ferreira-Aparicio, M. Abon, J.C. Volta, Catal. Today 32 (1996) 223.
[32] P.L. Gai-Boyes, Catal.: Rev. Sci. Eng. 34 (1992) 1.
[33] W.V. Schulmayer, H.M. Ortner, Int. J. Refract. Met. H 20 (2002) 261.
[34] H. Schmalzried, Solid State Reactions, Verlag Chemie, Weinheim, 1981, p. 197.
[35] J. Haber, J. Less Common Met. 54 (1977) 243.
[36] S. Rashid, P. Barnes, J. Bensted, X. Turrillas, J. Mater. Sci. Lett. 13 (1994) 1232.
[37] A.C. Jupe, X. Turrillas, P. Barnes, S.L. Colston, C. Hall, D. Häusermann, M. Hanfland, Phys. Rev. B (Rapid Commun.) 53 (1996) 14697.
[38] V.E. Heinrich, P.A. Cox, The Surface Science of Metal Oxides, Cambridge University Press, 1996, p. 118.
[39] A. Papakondylis, P. Sautet, J. Phys. Chem. 100 (1996) 10681.
[40] T. Ressler, J. Phys. Chem. B 106 (2002) 7719.
[41] P. Barnes, X. Turrilas, A.C. Jupe, S.L. Colston, D.O. O'Connor, R.J. Cernik, P. Livesey, C. Hall, D. Bates, R. Dennis, J. Chem. Soc. Faraday Trans. 92 (1996) 2187.
[42] P.B. Himelfarb, F.E. Wawner Jr., A. Bieser Jr., S.N. Vines, J. Catal. 83 (1983) 469.